Science of the Total Environment 739 (2020) 140361

Contents lists available at ScienceDirect

Science of the Total Environment

journal homepage: www.elsevier.com/locate/scitotenv

Spatiotemporal changes of surface solar radiation: Implication for air pollution and rice yield in East China

Yanyu Wang [a], Ze Meng [b], Rui Lyu [a], Guan Huang [c], Qianshan He [d,e,*], Tiantao Cheng [f,g,h,**]

[a] Shanghai Key Laboratory of Atmospheric Particle Pollution and Prevention (LAP3), Department of Environmental Science and Engineering, Institute of Atmospheric Sciences, Fudan University, Shanghai 200438, China
[b] School of Oceanography, Shanghai Jiao Tong University, Shanghai 200030, China
[c] College of Environmental Science and Engineering, Donghua University, Shanghai 201620, China
[d] Shanghai Meteorological Service, Shanghai 200030, China
[e] Shanghai Key Laboratory of Meteorology and Health, Shanghai 200030, China
[f] Department of Atmospheric and Oceanic Sciences, Institute of Atmospheric Sciences, Fudan University, Shanghai 200438, China
[g] Big Data Institute for Carbon Emission and Environmental Pollution, Fudan University, Shanghai 200438, China
[h] Shanghai Institute of Eco-Chongming (SIEC), Shanghai 200062, China

HIGHLIGHTS

- AOD dominates SSR transitions in East China during 2000–2016.
- The contribution of SSA to SSR becomes increasingly important with AOD increase.
- Observation evidences imply PBL regulates SSR in air pollution.
- Aerosol-induced reduction in radiation leads to 6.74% reduction in rice yield.

GRAPHICAL ABSTRACT

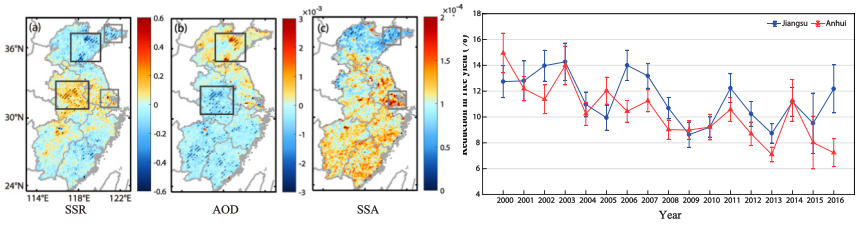

ARTICLE INFO

Article history:
Received 15 April 2020
Received in revised form 16 June 2020
Accepted 17 June 2020
Available online 20 June 2020

Editor: Pingqing Fu

Keywords:
Surface solar radiation
Aerosol pollution
Rice yield
WRF
SBDART

ABSTRACT

The changes of surface solar radiation (SSR) have significant implication for air pollution and rice yield. In this study, gridded SSR data, derived from multi-platform datasets and radiation model, were used to analyze its spatiotemporal changes over East China during 2000–2016. The results show SSR experiences dimming during 2000–2005, then turns into brightening till 2016. Both aerosol optical depth (AOD) and single scattering albedo (SSA) contribute to SSR trend. AOD dominates the spatiotemporal changes of SSR in East China, and this impact is higher in the North than the South. SSA has little impact on SSR with low AOD, but its contribution to SSR becomes important as AOD increases. Moreover, gridded planet boundary layer (PBL) was simulated by the Weather Research and Forecasting Model (WRF) and SSR-PBL relationship was also explored. Long-term evidence indicates PBL has a regulatory effect on SSR in the air pollution. Additionally, aerosol-induced radiation reduction can influence rice yield in East China, and it can result in about mean 6.74% reduction in rice yield over East China. Province-level changes of aerosol-induced reduction in rice production were also evaluated and it suggests the impact of aerosols on rice production is non-negligible, especially in Jiangsu and Anhui Province. Our study underscores the importance of aerosol pollution on surface radiation and the mitigation of aerosols is beneficial for crop production under climate change.

1. Introduction

Surface solar radiation (SSR) plays a vital role in the Earth-atmosphere system. It is the energy source of atmospheric circulation,

* Correspondence to: Q. He, Shanghai Meteorological Service, Shanghai 200030, China.
** Correspondence to: T. Cheng, Department of Atmospheric and Oceanic Sciences, Institute of Atmospheric Sciences, Fudan University, Shanghai 200438, China.
E-mail addresses: oxeye75@163.com (Q. He), ttcheng@fudan.edu.cn (T. Cheng).

https://doi.org/10.1016/j.scitotenv.2020.140361
0048-9697/

hydrological cycle and ecological environment (Ramanathan et al., 2001). SSR changes have profound influence on the surface temperature, air pollution as well as plants photosynthesis (Wild, 2012). Thus, a better understanding of SSR changes is critically important to regional climate, human health and crop production.

Previous studies have documented that SSR has undergone substantial decadal variations in recent years all over the world. Wild et al. (2005) reported SSR has shifted from decline ("solar dimming") between 1950s and 1980s to the increase ("solar brightening") during the 1990s. After 2000, a continuation of brightening in the developed regions, such as Europe, the United States and Korea (Wild et al., 2009). In China, the dimming levelled off in the 1980s, but did not turn into brightening until 2005 (Yang et al., 2018). Li et al. (2018) extended the analysis into 2005–2015 and concluded the solar brightening in recent few years in East China. Furthermore, various explanations were provided for the SSR trend in many studies (Wang et al., 2012; Qian et al., 2007). The change of anthropogenic aerosols is considered to be the most plausible explanation for SSR trend in the past ten years. It is acknowledged that aerosols can absorb and scatter solar radiation directly, they also affect cloud formations by acting as cloud condensation nuclei or ice nuclei, and clouds can further attenuate the incoming radiation (Rosenfeld, 1999). Apart from aerosols, other driving factors, such as clouds, wind speed and water vapor, are also reported to influence SSR variations in the regional scale (Wang and Yang, 2014). For example, Yang et al. (2012) suggested that the increase of water vapor amount and deep cloud cover are responsible for the dimming over Tibetan Plateau. Wang et al. (2014) found strong relationship between SSR and wind speed during 1961–2011 across China. Recently, Schwarz et al. (2020) pointed that SSR trend is not attributable to one single factor, it is the atmospheric absorption in clouds and aerosols driving the dimming/brightening in Europe and China. Apart from SSR variability, much attention is also paid to the role of SSR in the haze events in China. The reduction in SSR induced by cumulative aerosols is one of the most important characteristics in the aerosol pollution (Petäjä et al., 2016). In the heavy haze, surface measurements showed that hourly global radiant exposure can decreased up to 56% during aerosols cumulative stage (Zhong et al., 2018). When $PM_{2.5}$ concentrations are greater than 400 μg m^{-3}, owing to SSR reduction, the subsequent decrease in near-ground temperature can exceed −4 °C in Beijing (Zhong et al., 2019). These prior works have highlighted the importance of SSR variation not only in the long-term decades but also in the short haze cases.

With unprecedented socioeconomic development, East China has witnessed serious air pollution, aerosol emissions and aerosol compositions have large functions (Che et al., 2018; Wang et al., 2019). Accordingly, associated aerosol optical parameters, including aerosol optical depth (AOD) and single scattering albedo (SSA), produce complex influence on SSR variability. Many efforts have been devoted into the impact of AOD on SSR trend, such as Xia (2010) and Wang et al. (2012). Only few studies focus on the individual contribution of SSA to SSR trend. Qian et al. (2007) pointed that the increment of SSA since 1980s can result in the transition of SSR from a decreasing trend to no apparent trend. Li et al. (2018) suggested the increase of SSA can contribute to SSR by the increase of diffuse fraction in XiangHe Station in China. Moreover, the combined effect of AOD and SSA to SSR variation was not fully understood. In addition, previous studies only focus on the sudden decrease of SSR in the specific haze event, long-term performance of SSR in the air pollution were barely addressed due to lack of continuous aerosol and radiation data. Based on this, high-accuracy and fine-resolution SSR dataset was retrieved under clear-sky using radiation transfer model and multi-platform datasets, including the MODerate Resolution Imaging Spectroradiometer (MODIS), Clouds and the Earth's Radiant Energy System (CERES) and the Modern-Era Retrospective Analysis for Research and Application, version 2 (MERRA-2). Meanwhile, these datasets also provide long-term AOD and SSA information, which can be used to evaluate their contributions to SSR trend in East China. Compared with surface measurements, our datasets have advantages of full spatial and temporal coverage, and they can offer valuable information about full picture of SSR and aerosol optical properties, especially for the rural area with unavailable observations. Planet boundary layer (PBL) is often used as a proxy for unfavorable meteorological conditions and shallow PBL is one of the critical characteristics in air pollution (Wang et al., 2018). Long-term gridded PBL, simulated by the Weather Research and Forecasting Model (WRF), was used to examine the relationship with SSR in our study. Additionally, based on the radiation transfer model, the difference of SSR with and without aerosols can be simulated in each grid. This aerosol-induced reduction in SSR exerts significant influence on crop photosynthesis and crop yield, especially in East China, the main rice production area in China. It paves the way for quantitative evaluation of rice yield reduction in East China. Overall, the specific objectives in our study are (1) to examine SSR trend and its associated factors in East China during the past 16 years; (2) to explore the role of SSR in the air pollution; (3) to estimate the aerosol-induced reduction in rice production across East China. The paper is organized as follows. The data is described in Section 2, and Section 3 introduces the methodology. Section 4 discusses the SSR trend, SSR-PBL relationship in air pollution as well as the impact of aerosol-induced SSR reduction on rice yield in East China. The conclusion can be found in Section 5.

2. Data

Multi-platform datasets were used as inputs to the radiative transfer model to perform SSR simulation in East China. First, AOD was derived from MODIS Level 2 products over land (C6, 10-km resolution at the nadir) at Terra satellite (Levy et al., 2013). He et al. (2010) demonstrated that MODIS AOD was correlated with surface measurements (CE-318 sunphotometer) at 7 sites in China, with a correlation coefficient of 0.85 and 90% of cases falling in the range of $\Delta AOD = \pm 0.05 \pm 0.20$ AOD (Chu et al., 2002). Surface albedo comes from MODIS MCD43C3 black-sky albedo product (C6) in shortwave (0.3–5 μm) band. Hourly SSA product at 0.55 μm was acquired by MERRA-2. More detail information about MERRA-2 can be found in Randles et al. (2017). The validation reflected that MERRA-2 SSA has ±20% uncertainty in East China (Wang et al., 2020). ASY was retrieved by matching simulated radiative flux at the top of atmosphere (TOA) from transfer model and CERES observation, binary search method was used to find the ASY when simulated TOA flux is closest to CERES observation. Here, CERES Single Scanner Footprint (SSF) level 2 product at Terra satellite was used and can provide shortwave upward TOA radiative flux. The detailed algorithm and the uncertainty of ASY were discussed detailed in Wang et al. (2020). ERA-Interim (European Center for Medium-Range Weather Forecast (ECMWF) Interim Reanalysis) provides the total column ozone, total column water vapor and atmospheric profile data (temperature, water vapor density, and ozone density). The data quality of the ERA-Interim reanalysis data can be found in Dee et al. (2011). In addition, aerosol vertical profiles were also input to the transfer model to obtain more accurate SSR. It was derived from two-layer aerosol vertical distribution model proposed by He et al. (2008). The important parameters in this aerosol model is PBL, and it was simulated by a three-domain, two-way nested WRF Model (version 3.2.1), with 10 km resolution of innermost domain. The detailed retrieval of aerosol vertical profile can be found in He et al. (2016). In this study, these datasets were interpolated to a spatial resolution of $0.1° \times 0.1°$ to collocate with the MODIS/AOD data by bilinear interpolation. The SSR simulation was also performed in each $0.1° \times 0.1°$ grid over East China. For temporal resolution, AOD and TOA radiation fluxes were from MODIS and CERES sensor aboard the Terra satellite respectively, and they are available once per day. Both SSA and ERA-Interim are hourly means, surface albedo product in daily means. SSR simulations were performed only at the passing over of the Terra satellite under clear skies.

In addition, MODIS land cover type product (MCD12Q1, C6) was utilized to identify cropland grids in East China. International Geosphere-

Biosphere Program (IGBP) scheme can provide 17 land cover categories, including urban, cropland, grassland, water body, etc. Its temporal resolution is yearly and spatial resolution is 500 m. Here, a static land type map (MCD12Q1 product in 2008) was used to define the cropland grids in East China. In our study, cropland grid can be approximately considered as the rice area in East China, because rice is the main crop in East China. Fig. S1 shows the map of East China (114–124°E, 24–38°N), it also includes the terrain, major mountains and lakes in East China. The temporal coverage of our study is from 2000 to 2016.

3. Method

Clear-sky SSR in the shortwave (0.25–4 μm) spectral region was estimated by the Santa Barbara Discrete Atmospheric Radiative Transfer (SBDART) model (Ricchiazzi et al., 1998). This model has been widely used for the estimation of surface downward/upward irradiance and aerosol-induced variation in SSR (Tian et al., 2018a; Tian et al., 2018b). The main inputs of this model include aerosol properties (AOD from MODIS; SSA from MERRA-2; ASY from the retrieval), surface albedo (from MODIS), aerosol vertical profile (from WRF simulation), atmospheric profiles (from ECMWF), total column ozone and water vapor (from ECMWF). The main outputs are downward/upward radiative fluxes at the surface and TOA with and without aerosols. The downward surface radiative flux is SSR. The detail description of algorithm can be found in Wang et al. (2020). The validation showed simulated SSR was highly correlated with three pyranometer sites in East China during 2000–2014, with the correlation coefficient of over 0.87 (Wang et al., 2020). Following this method, long-term gridded SSR dataset during 2000–2016 can be obtained with a spatial resolution of 0.1° × 0.1°. Then SSR dataset, along with other aerosol optical parameters (AOD, SSA) and PBL, was used to investigate SSR trend in East China.

In addition, aerosol-induced changes of SSR can be calculated as:

$$\Delta F = \frac{F - F_0}{F_0} \times 100\% \quad (1)$$

where F and F_0 represent downward surface radiative fluxes with and without aerosols, respectively. Here, ΔF is negative, which represents

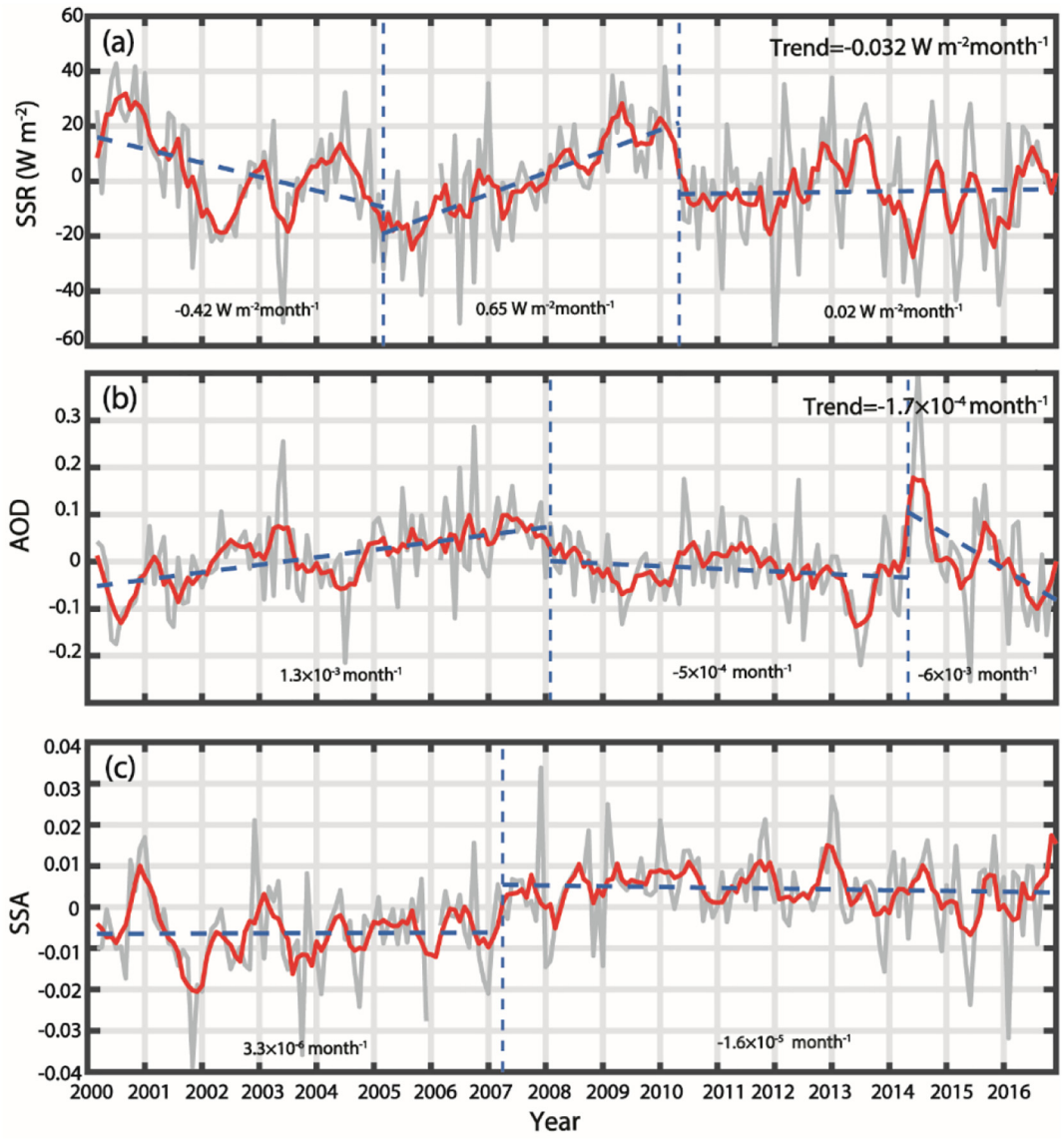

Fig. 1. Time series of monthly mean (a) SSR, (b) AOD and (c) SSA in East China during 2000–2016. Grey lines represent the deseasonalized time series, red lines denote 5-month moving average. Dashed blue lines are piecewise linear fits. The values of Mann-Kendall (MK) trend during the whole period (2000–2016) are shown in the top right corner and the trends during different period are in the bottom of the figure. Here, only statistically significant trends (>90%) are shown.

SSR reduction due to aerosol direct effect. It's noted that SSR attenuation can decrease the total Photosynthetically Active Radiation (PAR, 380–710 nm). Simultaneously, the diffuse fraction of PAR can increase, it is favorable to plant photosynthesis and partly offsets the negative effect of decreased total PAR (Greenwald et al., 2006). Considering these combined effects of total and diffuse PAR on rice photosynthesis, T. Zhang et al. (2017) derived the relationship between the changes of solar radiation (ΔF) and rice yield (ΔY) in East China (shown in Fig. S2) using the radiation transfer model (Column Radiation Model, CRM) and rice growth model (ORYZA, v3). The simulation showed there is a decrease in rice yield with lower SSR and a concurrent increase in yield with higher diffuse radiation. Based on the net effect of two contrasting processes, rice yield in East China still has a negative response to aerosol-induced SSR reduction. According the function of ΔF-ΔY and MODIS land cover type dataset, the changes of reduction in rice yield can be calculated in each cropland grid of East China.

To detect the turning point in the time series of SSR, AOD and SSA, a piecewise linear fit method as described in Rebecca et al. (2012) was implemented in our study. It can automatically detect multiple changepoints in large climate data records. In addition, temporal trends of SSR, and their significance levels (90%) were estimated by Sen's slope method (Sen, 1968) Mann-Kendall (MK) test (Mann, 1945; Kendall, 1975). More detailed description and analysis procedure can be found in Li et al. (2014). Prior to trend analysis, all the data were deseasonalized by subtracting the corresponding multi-year monthly mean during 2000–2016 in order to eliminate the effect of annual and seasonal cycles.

4. Results and discussion

4.1. SSR trend and its factors

Fig. 1 portrays the time series of monthly mean SSR, AOD and SSA anomalies in East China during 2000–2016 (deseasonalized, grey lines). 5-month moving average method was applied to remove the noise component from these time series (shown in red lines). To detect the turning point, piecewise linear fitting method was performed (Rebecca et al., 2012). The dashed blue line is the slope of least-squares-fit regression, and can represent temporal trend. As shown in Fig. 1a, SSR has a significant negative trend of -0.032 W m^{-2} month^{-1}, indicating East China actually has experienced dimming during past decades. Two turning points in SSR trend are detected, that is, the 63th and 125th month during the period of 2000–2016. SSR decreases by -0.42 W m^{-2} month^{-1} in East China during 2000–2005. Then it increases with the rate of 0.55 W m^{-2} month^{-1} until 2010. After that, SSR slows down and maintains at a steady rate of 0.02 W m^{-2} month^{-1}. This trend agrees well with Wild et al. (2009) and Yang et al. (2018). But the magnitude of our SSR trend is larger than the national mean (-0.42 W m^{-2} year^{-1}, Wild et al. (2009)) during 2000–2005. It's due to that East China experiences rapid economic growth and it's highly polluted, aerosol-induced SSR decline is larger than other regions in China. In Wild et al. (2009), Shanghai station showed a much larger decline trend and is consistent with our SSR trend, while SSR presented increase trend in some clean region, such as Kunming station. Another reason is that satellite-derived SSR is generally larger in magnitude than observation (Tang et al., 2011), because it is sensitive to satellite sensor calibration and clouds contamination.

The temporal trend of AOD (Fig. 1b) captures slightly negative over East China during 2000–2016. Specifically, there is an increase in AOD during 2000–2008, and subsequently a slight decrease until 2014. Then a pronounced decrease is found from 2014 to 2016. A similar shift of AOD trend in East China was also reported by J. Zhang et al. (2017) and Li (2020). It is mainly attributed to the changes of anthropogenic emissions over East China (Che et al., 2015). Explosive growth in emissions induced by economic development is responsible for AOD increase, and then after 2008, a series of effective emission controls result in the AOD reduction. Lu et al. (2011) found an increase of 62% in SO_2 emission in China during 2000–2006 then decreased by 9.2% during 2006–2010. Zheng et al. (2018) also estimated 59% decrease for SO_2 and 21% for NO_x during 2013–2017 based on emission inventory. Besides from emissions, the changes of meteorological condition also play a non-negligible role in AOD variations, especially concerning natural aerosols (Che et al., 2019a; Wang et al., 2019). Combined Fig. 1a and b, AOD exactly shared the reverse phase with SSR although the turning point is different. That is to say, drastic increase in AOD leads to SSR reduction during 2000–2005, and after that SSR increase is in response to AOD decline. Fig. 1c shows an increase of SSA from 2000 to 2007, and then followed by a slight decline. It has a good agreement with AERONET observation in China (Li et al., 2014). The changes of SSA may be closely related with the changes of anthropogenic emissions. The increase of SSA during 2000–2007 may suggest the absorbing aerosols, such as black carbon, decreased more than scattering aerosols. Additionally, SSA has strong dependence of aerosol size distribution. Zhuang et al. (2018) revealed coarse particles have weaker scattering than fine ones based on surface measurements in Nanjing. The increase fraction of large-size AOD is likely a consequence of the decrease of SSA after 2007 (Zhao et al., 2017). Generally, higher SSA means less absorption, consequently makes SSR increase on the assumption of the same amount of aerosols. Based on Fig. 1a and c, it is speculated that the increment of SSA during 2000–2007 seems to partly offset the decrease of SSR induced by AOD reduction, but the contribution of SSA is insignificant in East China.

For temporal SSR trend, it seems AOD dominated its variability in the past 16 years. To further examine the temporal relationship between SSR and AOD, temporal correlation coefficient (TCC) between SSR and AOD was calculated in Fig. 2. TCC is significant negative (90% significant level) in all grids and its absolute value is shown here for comparison. Mean correlation coefficient is -0.78. It is clear to see that SSR has an intimate inverse phase with AOD in the past decades. Compared with the southern area, higher correlation coefficients are found in the North, especially in Shandong Province, the northern areas of Jiangsu and Jiangxi. This implies that AOD is the leading factor of SSR trend in the North. But in the South, apart from AOD, there must be other potential factors influencing SSR trend (Che et al., 2019a, 2019b). The

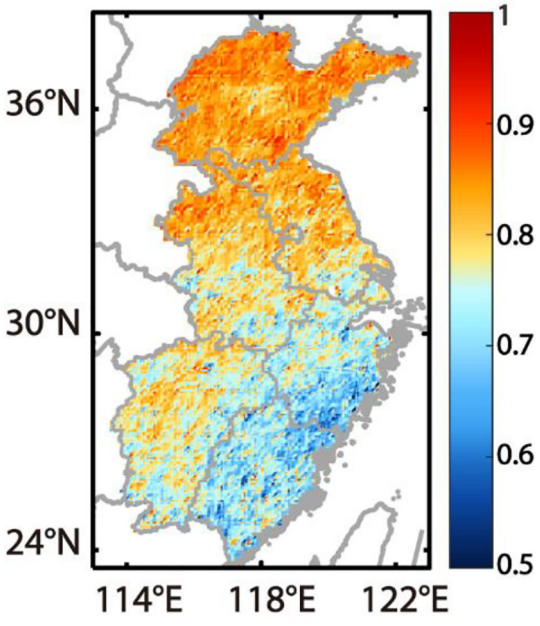

Fig. 2. Temporal correlation coefficients (TCC) between deseasonalized time series of SSR and AOD in each grid of East China during 2000–2016. All grids pass the 90% significant levels. The absolute value of TCCs is shown here.

apparent evidence was not found in TCC between SSR and SSA (not shown). In addition to AOD and SSA, it is speculated that the difference of relative humidity (RH) across East China may be responsible for the SSR trend in the South. He et al. (2016) found that RH is much higher in the South than the North. As Yang et al. (2009) demonstrated, RH has negative correlation with SSR, with the correlation coefficient of −0.64 in China. Wild et al. (2009) also pointed out that 10% increase in water vapor can attenuate SSR by 0.5%. High RH favors the hygroscopic growth of aerosol particles, can make the increase of aerosol extinction coefficient, and further attenuate SSR. An interesting phenomenon is found, TCC pattern seemingly resembles the terrain of East China (Fig. S1). The high terrain overlaps the area with low correlation between SSR and AOD. SSR trend in the South can presumably be associated with the complex underlying characteristics and surface albedo. However, the change of albedo induced by urbanization and deforestation is significant for upward radiation, but this impact is limited to the SSR variation (Wang et al., 2020). Here, more additional observation data are needed to further explore the difference in influential factors of SSR trend between the North and South of East China.

To figure out the contribution of AOD and SSA to SSR trend, a sensitivity test was performed using SBDART model. Fig. 3a displays SSR results with different ranges of AOD (0–1.0) and SSA (0.8–1.0). The enhancement of AOD can result in a sharp reduction in SSR with SSA fixed, in contrast, SSA increase leads to SSR increase. This quantitative result validated our speculation. Fig. 3b illustrates the response of SSR to SSA in different AOD. It's clear to see that, SSA has little impact on SSR when AOD is low, but when AOD is over 0.6, this impact tends to become significant. The black curve denotes the cumulative change of SSR with SSA varying 0.8–1.0. SSR change increases significantly with AOD increase. When AOD equals 1, the increase of SSR can be up to 180 W m^{-2}. In East China, it can be deduced that the contribution of SSA to SSR is larger in the North, because AOD is much higher in the North compared with the South.

Fig. 4 depicts the spatial MK trends of SSR, AOD and SSA across East China during 2000–2016. As displayed in Fig. 4a, black square in the eastern areas of Yimeng Mountain (Fig. S1) has solar dimming. These areas overlap the areas with large positive trends of AOD (Fig. 4b), demonstrating AOD dominated in SSR trend in this area. Meanwhile, obvious brightening is prevalent in the middle areas of East China, including Anhui Province and nearby the Poyang Lake of Jiangxi Province. This can be attributed by the significant negative AOD trend in these areas (Fig. 4b). Yangtze River Delta (YRD) Region (118–123°E, 29–33°N) experiences brightening (Fig. 4a), positive SSA trend can compensate SSR reduction induced by AOD increased in this region (Fig. 4b), and can be partly explained the brightening. Similarly, negative SSA trend in the eastern Shandong Province can be an explanation for negative SSR trend in this region. In summary, the combined effect of AOD and SSA contribute to the spatial trend of SSR in East China.

4.2. SSR-PBL relationship in the air pollution

Previous studies have observed a sharp reduction of SSR in severe air pollution, and SSR plays a vital role in the aerosol-PBL interaction (Miao et al., 2019). To explore the role of SSR in air pollution, long-term relationship among SSR, AOD and PBL in four seasons during 2000–2016 was examined and shown in Fig. 5. Mean AOD is calculated based on the different ranges of SSR and PBL. Noted that SSR range is different in four seasons, this is because SSR has a seasonal cycle, with high value in summer and low in winter. AOD can be considered as an indicator of aerosol pollution. According to He et al. (2012), high AOD (>1) represents heavy aerosol pollution, AOD <1 and AOD >0.5 is moderate aerosol pollution, and AOD <0.5 is clean and no-aerosol pollution. Fig. 5 reveals high AOD (>1, red color) is always accompanied by low SSR in four seasons, and it is consistent with our above findings. Model simulations suggested that monthly mean reductions of SSR in the heavy haze can be up to 13.5% (April, spring), 28.8% (July, summer), 23.6% (October, autumn) and 34.5% (January, winter) respectively in North China during the heavy haze events (Zhang et al., 2019). PBL is not sensitive to high AOD in spring (Fig. 5a) and summer (Fig. 5b). However, in autumn (Fig. 5c) and winter (Fig. 5d), PBL becomes shallower in response to high AOD, even drop to the below of 800 m. It is due to the different mechanism of pollution formations in four seasons. Air pollution in summer is mainly driven by emission, unfavorable meteorological factors, including low PBL, rarely participants in the formation of air pollution (Stirnberg et al., 2020). In contrast, almost all the winter haze events are caused by the combined effect of emission and meteorology. The different performances of PBL in spring and winter were also identified in Wang et al. (2016). Our statistical evidence demonstrates air pollution (high AOD) is always accompanied by both low SSR and shallow PBL in autumn and winter. In fact, there exists two-way feedback in this process (Miao et al., 2019). On the one hand, high AOD is often closely associated with stable atmospheric stratification, calm winds and shallow PBL. On the other hand, high concentrations of aerosols can enhance the stability of atmosphere and in turn decrease PBL, further exacerbate the pollution and consequently make SSR decrease more. In this process, it is pointed out the reduced SSR might suppress the photochemical oxidation process of aerosols, further hindering the formation of secondary aerosols. This may mitigate the aerosol pollution induced by PBL collapse. Meteorology-chemistry-radiation coupled model is further needed to explore the role of SSR and PBL in the aerosol pollution.

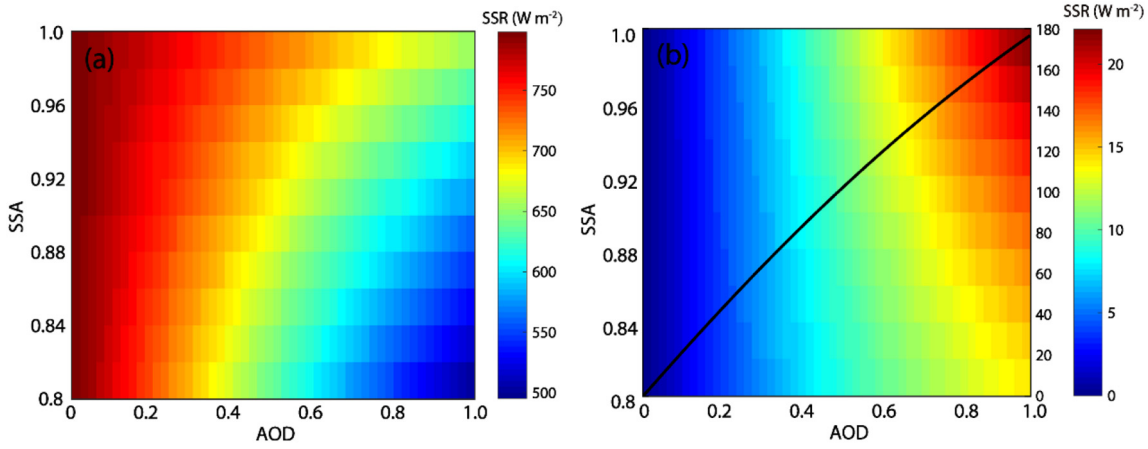

Fig. 3. Dependence of SSR on AOD and SSA in the sensitivity test. (a) SSR distribution in different AOD (0–1.0) and SSA (0.8–1.0), both intervals are 0.02. (b) The changes of SSR with SSA varying 0.02 in different AOD. The black curve represents the cumulative changes of SSR with SSA ranging from 0.8 to 1.0.

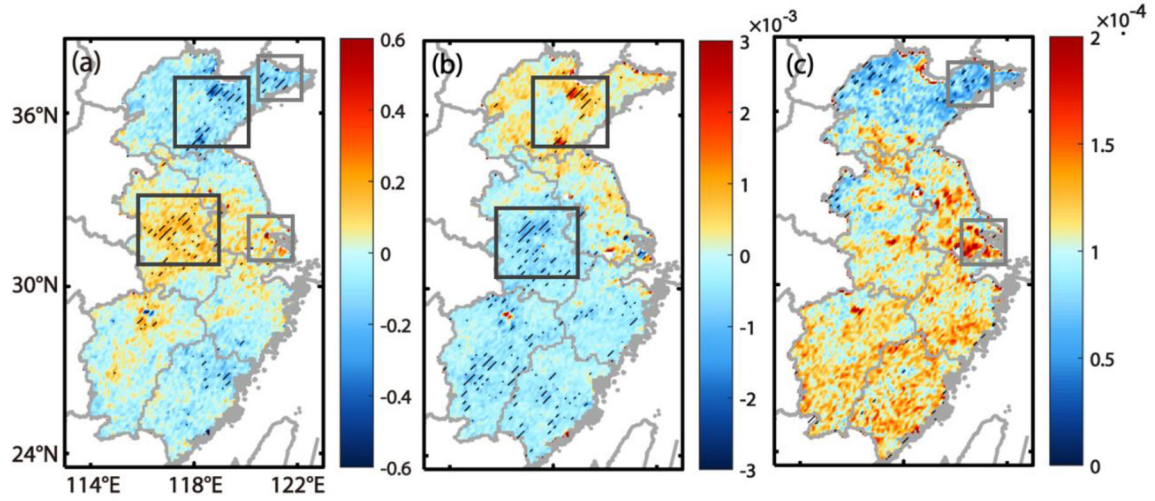

Fig. 4. Spatial MK trends of (a) SSR (W m^{-2} $month^{-1}$), (b) AOD ($month^{-1}$) and (c) SSA ($month^{-1}$) during 2000–2016 in East China. Hatched regions indicate the trend is above 90% significance level. Black squares are outlined for comparison between (a) SSR and (b) AOD. Similarly, grey squares are used to compare (a) SSR and (c) SSA.

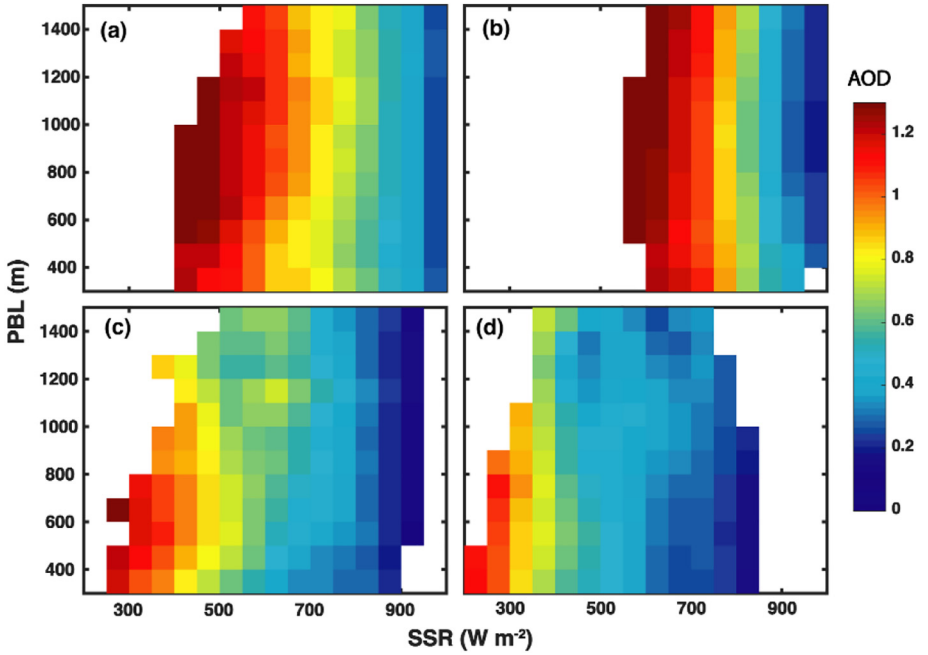

Fig. 5. Dependence of AOD on SSR and planet boundary layer (PBL) in (a) spring (March–May), (b) summer (June–August), (c) autumn (September–November), (d) winter (December–February). All the precipitation events were excluded to rule out the effect of wet deposition. (For interpretation of the references to color in this figure, the reader is referred to the web version of this article.)

For purpose of addressing SSR-PBL relationship, Fig. 6 displays the seasonal correlation coefficients between SSR and PBL in different AOD ranges. In spring (Fig. 6a) and summer (Fig. 6b), the coefficients are all less than 0.3, suggesting that the relationship between SSR and PBL seems not prominent. However, in autumn (Fig. 6c), this relationship turns to be intimate (correlation coefficient > 0.4) with AOD > 0.5. PBL reduction can apparently hinder the dispersion of aerosols and make SSR decline. Ding et al. (2013) proved that agricultural burning plumes in autumn can result in a decrease in the solar radiation intensity by more than 70% and modify the PBL environment. The intensive activities of straw burning in autumn may contribute to the formation of this PBL-SSR relationship (Tang et al., 2020). Fig. 6d also describes the similar behavior in winter, and it indicates PBL has an increasing effect on SSR with the aggravation of air pollution. In other words, air pollution can push PBL to be a regulator of SSR by controlling the dispersion of aerosols.

4.3. The implication for rice yield

Crop growth mainly depends on sunlight, water, and fertilization. The insufficiency of solar radiation can reduce the efficiency of plant photosynthesis according to the function between solar radiation (ΔF) and rice yield (ΔY) (Fig. S2). Fig. 7a displays mean distribution of aerosol-induced reduction in SSR across East China during 2000–2016. The acquired radiation during the growing season is key for rice growth, and thus SSR reduction during the growing season (3-month before the harvest time) was calculated in this study. Moreover, the different growing season of rice in different provinces of East China was also

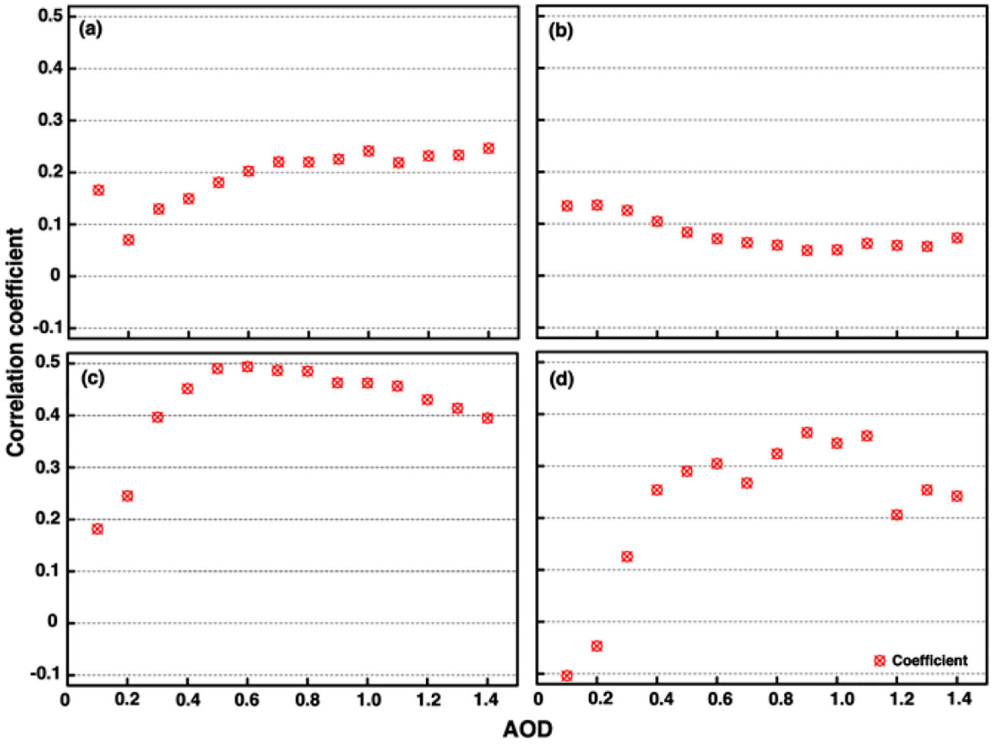

Fig. 6. The scatter plots of correlation coefficient between SSR and PBL in (a) spring, (b) summer, (c) autumn, (d) winter in different AOD ranges during 2000–2016. All the dots pass the 90% confidence level.

considered. As shown in Fig. 7a, aerosol-induced SSR reduction ranges from 2% to 30%, the mean value is 13.03% in East China. SSR reduction is larger in the North comparable with the South, especially in the west of Shandong Province, YRD and Poyang Lake Plain. Low value is observed in the southern Zhejiang and Fujian Province. This pattern is similar with AOD spatial distribution in East China, and the areas with high SSR reduction are also highly polluted. Meanwhile, the pattern with high SSR reduction also exactly overlaps the major crop production area in East China. Fig. 7b presents the mean estimated reduction of rice yield in East China during 2000–2016. SSR reduction only in cropland grids was calculated. Fig. S3 shows the distribution of land cover type in East China. The croplands are mainly dominated in the North, especially in Shandong, Jiangxi and Anhui Province. Some spare croplands are also found in the South due to the fragmentation of mountains. Mean reduction of rice yield is estimated about 6.74%, and large yield reduction occurs in the north and west of Yimeng Mountain. Meanwhile, 10.06% grids have less than 5% reduction, which is mainly found in the middle and eastern Shandong Province, and northern Anhui Province. Our result is similar to Tie et al. (2016), with 6% reduction in rice production in YRD. Chameides et al. (1999) also reported 3–30% yield improvement by mitigating aerosol pollution in China. Nevertheless, the result is not definitive answer, because our SSR reduction was estimated based on the assumption of 100% aerosol reduction. It's an ideal case with no aerosols in the atmosphere. Actually, the impact of aerosols on rice production is far smaller than this value. Overall, our results suggest air pollution exerts significant negative effect on rice yield in East China, especially in the severely polluted areas.

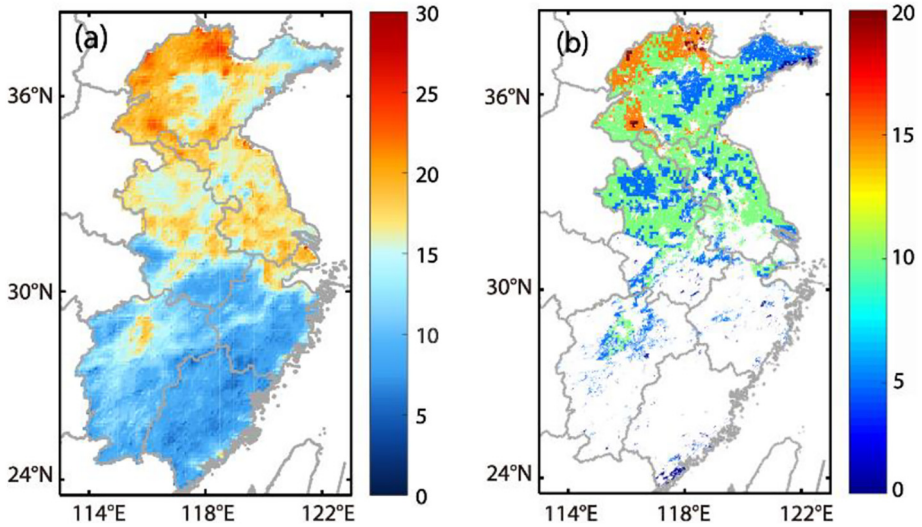

Fig. 7. The distribution of aerosol-induced reduction in (a) SSR and (b) rice yield. Here, the absolute percent of reduction is shown (unit: %).

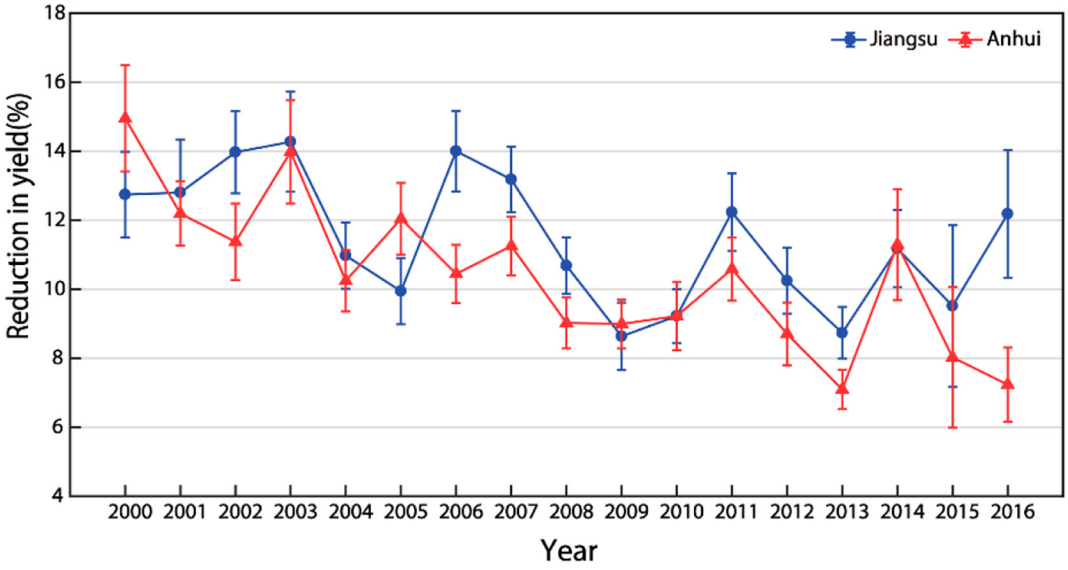

Fig. 8. Evolution of annual mean reduction in rice yield induced by aerosols in Jiangsu and Anhui Province from 2000 to 2016 (unit: %). Blue line represents Jiangsu Province and red line is Anhui Province.

According to province-level rice production in the Chinese Statistical Year (http://www.stats.gov.cn/tjsj/ndsj/), the top two rice production in East China is Jiangsu and Anhui Province. Fig. 8 reflects the changes of annual mean reduction in rice yield in these two provinces during 2000–2016. Blue line represents Jiangsu and red is Anhui Province. Reductions of rice yield in Jiangsu and Anhui both show fluctuation patterns, and mean reduction in net rice yield is 11.44% in Jiangsu and 10.39% in Anhui, respectively. This suggests that the impact of air pollution on rice production cannot be negligible, especially in the major rice production provinces. Apart from SSR, aerosols also influence the temperature, precipitation and climate. The changes of temperature and precipitation also produce additional effect on rice production under climate warming. As Zhang et al. (2010) demonstrated, the solar radiation and temperature are both positively correlated with rice yield in the most measurement stations of China.

5. Conclusion

Based on the long-term gridded SSR datasets, temporal and spatial trends of clear-sky SSR was firstly portrayed in East China. During 2000–2016, SSR experiences dimming during 2000–2005, and turns into the brightening until 2010, and after that, it keeps slightly brightening. The spatial inhomogeneity of SSR trend displays that SSR trend is positive in the middle of East China especially along with the Yangtze River, while the decreasing trend is found in the northern and southern areas, including the Shandong and Fujian Province. Both temporal and spatial comparisons between SSR and AOD reveal that AOD is the leading driver in the changes of SSR, and the impact of AOD on SSR is larger than the North compared with the South. Additionally, SSA is found to have minor influence on SSR when AOD is low, but it can contribute much larger to SSR with high AOD. Long-term statistical evidence shows that high AOD is always accompanied by reduced SSR and shallow PBL in autumn and winter. Furthermore, high correlation between PBL and SSR can exceed 0.4 when AOD is over 0.5, implying that air pollution is pushing PBL to regulate SSR. Finally, the distribution of aerosol-induced reduction in radiation was presented across East China. This reduction of solar radiation can depress 6.74% rice yield in East China. The areas with large reduction in rice yield exactly overlap the areas with heavy aerosol pollution. The province-level changes of yield reduction were also provided in Jiangsu and Anhui Province during 2000–2016. This indicates the mitigation of air pollution is indeed beneficial to improve the crop production.

Overall, this study outlines a full picture of SSR changes in the last decades under the background of air pollution and it has important implication for rice yield. Our study enriches the existing understanding of SSR variations, and valuable information on the solar dimming/brightening is provided, especially in the areas with unavailable observations. In this study, the regulatory effect of PBL on SSR is needed to further quantify based on meteorology-chemistry-radiation coupled model, more additional observation data are used to identify the different roles of SSR and PBL. Additionally, diffuse radiation is not considered in the estimation of rice yield reduction. Aerosol can make the total radiation reduction, and meanwhile, aerosols also partially change direct solar radiation to diffuse radiation. The increase of diffuse radiation may contribute to increase photosynthesis (Mercado et al., 2009). According to Yue and Unger (2018), the ratio of direct/diffuse radiation relays on the clouds, AOD, etc. Moderate AOD can increase diffuse radiation, but dense aerosol loadings suppress the plant photosynthesis due to the strong attenuation of total radiation. Therefore, aerosol-induced reduction in radiation still plays a negative role in rice production due to high AOD in East China. Additionally, Zhou et al. (2017) found the wheat and corn yield is more sensitive to aerosols compared with rice. From this point, the impact of aerosols on other crop production in East China needs more exploration.

CRediT authorship contribution statement

Yanyu Wang: Conceptualization, Methodology, Writing - original draft. **Ze Meng:** Visualization, Writing - review & editing. **Rui Lyu:** Data curation, Formal analysis. **Guan Huang:** Data curation, Formal analysis. **Qianshan He:** Supervision, Writing - review & editing. **Tiantao Cheng:** Supervision, Writing - review & editing.

Declaration of competing interest

The authors declare that they have no known competing financial interests or personal relationships that could have appeared to influence the work reported in this paper.

Acknowledgement

This research is supported by the National Natural Science Foundation of China (41775129, 41801367, and 41905131), the National Key Research and Development Program of China (2017YFC1501701, 2017YFC1501405, and 2016YFC0202003).

Appendix A. Supplementary data

Supplementary data to this article can be found online at https://doi.org/10.1016/j.scitotenv.2020.140361.

References

Chameides, W., Yu, H., Liu, S.C., Bergin, M., Zhou, X., Mearns, L., Wang, G., Kiang, C.S., Saylor, R.D., Luo, C., Huang, Y., Steiner, A., Giorgi, F., 1999. Case study of the effects of atmospheric aerosols and regional haze on agriculture: an opportunity to enhance crop yields in China through emission controls? Proc. Natl. Acad. Sci. U. S. A. 96 (24), 13626–13633. https://doi.org/10.1073/pnas.96.24.13626.

Che, H., Zhang, X.-Y., Xia, X., Goloub, P., Holben, B., Zhao, H., Wang, Y., Zhang, X.-C., Wang, H., Blarel, L., Damiri, B., Zhang, R., Deng, X., Ma, Y., Wang, T., Geng, F., Qi, B., Zhu, J., Yu, J., Chen, Q., Shi, G., 2015. Ground-based aerosol climatology of China: aerosol optical depths from the China Aerosol Remote Sensing Network (CARSNET) 2002–2013. Atmos. Chem. Phys. 15, 7619–7652. https://doi.org/10.5194/acp-15-7619-2015.

Che, H., Qi, B., Zhao, H., Xia, X., Eck, T.F., Goloub, P., Dubovik, O., Estelles, V., Cuevas-Agulló, E., Blarel, L., Wu, Y., Zhu, J., Du, R., Wang, Y., Wang, H., Gui, K., Yu, J., Zheng, Y., Sun, T., Chen, Q., Shi, G., Zhang, X., 2018. Aerosol optical properties and direct radiative forcing based on measurements from the China Aerosol Remote Sensing Network (CARSNET) in eastern China. Atmos. Chem. Phys. 18, 405–425. https://doi.org/10.5194/acp-18-405-2018.

Che, H., Gui, K., Xia, X., Wang, Y., Holben, B.N., Goloub, P., Cuevas-Agulló, E., Wang, H., Zheng, Y., Zhao, H., Zhang, X., 2019a. Large contribution of meteorological factors to inter-decadal changes in regional aerosol optical depth. Atmos. Chem. Phys. 19, 10497–10523. https://doi.org/10.5194/acp-19-10497-2019.

Che, H., Xia, X., Zhao, H., Dubovik, O., Holben, B.N., Goloub, P., Cuevas-Agulló, E., Estelles, V., Wang, Y., Zhu, J., Qi, B., Gong, W., Yang, H., Zhang, R., Yang, L., Chen, J., Wang, H., Zheng, Y., Gui, K., Zhang, X., Zhang, X., 2019b. Spatial distribution of aerosol microphysical and optical properties and direct radiative effect from the China Aerosol Remote Sensing Network. Atmos. Chem. Phys. 19, 11843–11864. https://doi.org/10.5194/acp-19-11843-2019.

Chu, D.A., Kaufman, Y.J., Ichoku, C., Remer, L.A., Tanré, D., Holben, B.N., 2002. Validation of MODIS aerosol optical depth retrieval over land. Geophys. Res. Lett. 29, 1617–1621. https://doi.org/10.1029/2001gl013205.

Dee, D.P., Uppala, S.M., Simmons, A.J., Berrisford, P., Poli, P., Kobayashi, S., Andrae, U., Balmaseda, M.A., Balsamo, G., Bauer, P., Bechtold, P., Beljaars, A.C.M., van de Berg, L., Bidlot, J., Bormann, N., Delsol, C., Dragani, R., Fuentes, M., Geer, A.J., Haimberger, L., Healy, S.B., Hersbach, H., Hólm, E.V., Isaksen, L., Kållberg, P., Köhler, M., Matricardi, M., Mc-Nally, A.P., Monge-Sanz, B.M., Morcrette, J.J., Park, B.K., Peubey, C., de Rosnay, P., Tavolato, C., Thépaut, J.-N., Vitart, F., 2011. The ERA reanalysis: configuration and performance of the data assimilation system. Q. J. R. Meteorol. Soc. 137, 553–597. https://doi.org/10.1002/qj.828.

Ding, A.J., Fu, C.B., Yang, X.Q., Sun, J.N., Petäjä, T., Kerminen, V.-M., Wang, T., Xie, Y., Herrmann, E., Zheng, L.F., Nie, W., Liu, Q., Wei, X.L., Kulmala, M., 2013. Intense atmospheric pollution modifies weather: a case of mixed biomass burning with fossil fuel combustion pollution in eastern China. Atmos. Chem. Phys. 13, 10545–10554. https://doi.org/10.5194/acp-13-10545-2013.

Greenwald, R., Bergin, M.H., Xu, J., Cohan, D., Hoogenboom, G., Chameides, W.L., 2006. The influence of aerosols on crop production: a study using the CERES crop model. Agric. Syst. 89 (2–3), 390–413. https://doi.org/10.1016/j.agsy.2005.10.004.

He, Q., Li, C., Mao, J., Lau, A., Chu, D., 2008. Analysis of aerosol vertical distribution and variability in Hong Kong. J. Geophys. Res. 113, D14211. https://doi.org/10.1029/2008JD009778.

He, Q., Li, C., Tang, X., Li, H., Geng, F., Wu, Y., 2010. Validation of MODIS derived aerosol optical depth over the Yangtze River Delta in China. Remote Sens. Environ. 114, 1649–1661. https://doi.org/10.1016/j.rse.2010.02.015.

He, Q., Li, C., Geng, F., Lei, Y., Li, Y., 2012. Study on long-term aerosol distribution over the land of East China using MODIS data. Aerosol Air Qual. Res. 12, 300–315. https://doi.org/10.4209/aaqr.2011.11.0200.

He, Q., Li, C., Geng, F., Zhou, G., Gao, W., Yu, W., Li, Z., Du, M., 2016. A parameterization scheme of aerosol vertical distribution for surface-level visibility retrieval from satellite remote sensing. Remote Sens. Environ. 181, 1–13. https://doi.org/10.1016/j.rse.2016.03.016.

Kendall, M.G., 1975. Rank Correlation Methods. Griffin, London (160 pp).

Li, J., 2020. Pollution trends in China from 2000 to 2017: a multi-sensor view from space. Remote Sens. 12, 208. https://doi.org/10.3390/rs12020208.

Li, J., Carlson, B.E., Dubovik, O., Lacis, A.A., 2014. Recent trends in aerosol optical properties derived from AERONET measurements. Atmos. Chem. Phys. 14, 12271–12289. https://doi.org/10.5194/acp-14-12271-2014.

Li, J., Jiang, Y.W., Xia, X., Hu, Y.Y., 2018. Increase of surface solar irradiance across East China related to changes in aerosol properties during the past decade. Environ. Res. Lett. 13, 034006. https://doi.org/10.1088/1748-9326/aaa35a.

Lu, Z., Zhang, Q., Streets, D.G., 2011. Sulfur dioxide and primary carbonaceous aerosol emissions in China and India, 1996–2010. Atmos. Chem. Phys. 11, 9839–9864. https://doi.org/10.5194/acp-11-9839-2011.

Mann, H.B., 1945. Nonparametric tests against trend. Econometrica 13, 245–259.

Mercado, L.M., Bellouin, N., Sitch, S., Boucher, O., Huntingford, C., Wild, M., Cox, P., 2009. Impact of changes in diffuse radiation on the global land carbon sink. Nature 458, 1014–1018. https://doi.org/10.1038/nature07949.

Miao, Y.C., Li, J., Miao, S.G., Che, H.Z., Wang, Y.Q., Zhang, X.Y., Zhu, R., Liu, S.H., 2019. Interaction between planetary boundary layer and PM2.5 pollution in megacities in China: a review. Curr. Pollut. Rep. https://doi.org/10.1007/s40726-019-00124-5.

Petäjä, T., Järvi, L., Kerminen, V.-M., Ding, A.J., Sun, J.N., Nie, W., Kujansuu, J., Virkkula, A., Yang, X.Q., Fu, C.B., Zilitinkevich, S., Kulmala, M., 2016. Enhanced air pollution via aerosol-boundary layer feedback in China. Sci. Rep. 6 (1), 18998. https://doi.org/10.1038/srep18998.

Qian, Y., Wang, W., Leung, L.R., Kaiser, D.P., 2007. Variability of solar radiation under cloud-free skies in China: the role of aerosols. Geophys. Res. Lett. 34, L12804. https://doi.org/10.1029/2006GL028800.

Ramanathan, V., Crutzen, P.J., Kiehl, J.T., Rosenfeld, D., 2001. Aerosols, climate, and the hydrological cycle. Science 294, 2119–2124. https://doi.org/10.1126/science.1064034.

Randles, C.A., Sliva, A.M.D., Buchard, V., Colarco, P.R., Flynn, C.J., 2017. The MERRA-2 aerosol reanalysis, 1980–onward, part I: system description and data assimilation evaluation. J. Clim. 30, 6823. https://doi.org/10.1175/JCLI-D-16-0609.1.

Rebecca, K., Paul, F., Eckley, Idris A., 2012. Optimal detection of changepoints with a linear computational cost. J. Am. Stat. Assoc. 107 (500), 1590–1598.

Ricchiazzi, P., Yang, S.R., Gautier, C., Sowle, D., 1998. SBDART: a research and teaching software tool for plane parallel radiative transfer in the Earth's atmosphere. B. Am. Meteorol. Soc. 79, 2101–2114. https://doi.org/10.1175/1520-0477(1998)0792.0.CO;2.

Rosenfeld, D., 1999. TRMM observed first direct evidence of smoke from forest fires inhibiting rainfall. Geophys. Res. Lett. 26, 3105–3108. https://doi.org/10.1029/1999gl006066.

Schwarz, M., Folini, D., Yang, S., Allan, R.P., Wild, M., 2020. Changes in atmospheric shortwave absorption as important driver of dimming and brightening. Nat. Geosci. 13, 110–115. https://doi.org/10.1038/s41561-019-0528-y.

Sen, P.K., 1968. Estimates of the regression coefficient based on Kendall's tau. J. Am. Stat. Assoc. 63, 1379–1389.

Stirnberg, R., Cermak, J., Fuchs, J., Andersen, H., 2020. Mapping and understanding patterns of air quality using satellite data and machine learning. J. Geophys. Res. 125. https://doi.org/10.1029/2019JD031380.

Tang, W.J., Yang, K., Qin, J., Cheng, C.C.K., He, J., 2011. Solar radiation trend across China in recent decades: a revisit with quality-controlled data. Atmos. Chem. Phys. 11, 393–406. https://doi.org/10.5194/acp-11-393-2011.

Tang, R., Huang, X., Zhou, D., Ding, A., 2020. Biomass-burning-induced surface darkening and its impact on regional meteorology in eastern China. Atmos. Chem. Phys. 20, 6177–6191. https://doi.org/10.5194/acp-20-6177-2020.

Tian, P., Zhang, L., Cao, X., Sun, N., Wang, H., 2018a. Enhanced bottom-of-the-atmosphere cooling and atmosphere heating efficiency by mixed-type aerosols: a classification based on aerosol nonsphericity. J. Atmos. Sci. 75, 113–124. https://doi.org/10.1175/JAS-D-17-0019.1.

Tian, P., Zhang, L., Ma, J., Tang, K., Xu, L., Wang, Y., Cao, X., Liang, J., Ji, Y., Jiang, J.H., Yung, Y.L., Zhang, R., 2018b. Radiative absorption enhancement of dust mixed with anthropogenic pollution over East Asia. Atmos. Chem. Phys. 18, 7815–7825. https://doi.org/10.5194/acp-18-7815-2018.

Tie, X., Huang, R., Dai, W., Cao, J., Long, X., Su, X., Zhao, S., Wang, Q., Li, G., 2016. Effect of heavy haze and aerosol pollution on rice and wheat productions in China. Sci. Rep. 6, 29612. https://doi.org/10.1038/srep29612.

Wang, Y.W., Yang, Y.H., 2014. China's dimming and brightening: evidence, causes and hydrological implication. Ann. Geophys. 32, 41–55. https://doi.org/10.5194/angeo-32-412014.

Wang, K.C., Dickinson, R.E., Wild, M., Liang, S., 2012. Atmospheric impacts on climatic variability of surface incident solar radiation. Atmos. Chem. Phys. 12, 9581–9592. https://doi.org/10.5194/acp-12-9581-2012.

Wang, Y., Yang, Y., Zhou, X., Zhao, N., Zhang, J., 2014. Air pollution is pushing wind speed into a regulator of surface solar irradiance in China. Environ. Res. Lett. 9, 054004. https://doi.org/10.1088/1748-9326/9/5/054004.

Wang, X., Wang, K.C., Su .Y., L., 2016. Contribution of atmospheric diffusion conditions to the recent improvement in air quality in China. Sci. Rep. 6, 36404. https://doi.org/10.1038/srep36404.

Wang, X., Dickinson, R., Su, L., Zhou, C., Wang, K., 2018. PM2.5 pollution in China and how it has been exacerbated by terrain and meteorological conditions. B. Am. Meteorol. Soc. 99, 105–120. https://doi.org/10.1175/BAMS-D-16-0301.1.

Wang, Y., Duan, J., Xie, X., He, Q., Cheng, T., Mu, H., Gao, W., Li, X., 2019. Climatic factors and their availability in estimating long-term variations of fine particle distributions over East China. J. Geophys. Res. Atmos. 124. https://doi.org/10.1029/2018JD029622.

Wang, Y., Lyu, R., Xie, X., Huang, M., Wu, J., Mu, H., Yu, Q.R., He, Q., Cheng, T., 2020. Retrieval of gridded aerosol direct radiative forcing based on multiplatform datasets. Atmos. Meas. Tech. 13, 575–592. https://doi.org/10.5194/amt-13-575-2020.

Wild, M., 2012. Enlightening global dimming and brightening. B. Am. Meteorol. Soc., 27–37 https://doi.org/10.1175/BAMS-D-11-00074.1.

Wild, M., Trüssel, B., Ohmura, A., Long, C.N., König-Langlo, G., Dutton, E.G., Tsvetkov, A., 2009. Global dimming and brightening: an update beyond 2000. J. Geophys. Res. 114, D00D13. https://doi.org/10.1029/2008JD011382.

Xia, X., 2010. A closer looking at dimming and brightening in China during 1961–2005. Ann. Geophys. 28, 1121–1132. https://doi.org/10.5194/angeo-28-1121-2010.

Yang, Y.H., Zhao, N., Hao, X.H., Li, C.Q., 2009. Decreasing trend of sunshine hours and related driving forces in North China. Theor. Appl. Climatol. 97, 91–98. https://doi.org/10.1007/s00704-008-0049-x.

Yang, K., Ding, B., Qin, J., Tang, W., Lu, N., Lin, C., 2012. Can aerosol loading explain the solar dimming over the Tibetan Plateau? Geophys. Res. Lett. 39, L20710. https://doi.org/10.1029/2012GL053733.

Yang, S., Wang, X., Wild, M., 2018. Homogenization and trend analysis of the 1958–2016 in situ surface solar radiation records in China. J. Clim. 31, 4529–4541. https://doi.org/10.1175/JCLI-D-17-0891.1.

Yue, X., Unger, N., 2018. Fire air pollution reduces global terrestrial productivity. Nat. Commun. 9, 5413. https://doi.org/10.1038/s41467-018-07921-4.

Zhang, T., Zhu, J., Wassmann, R., 2010. Responses of rice yields to recent climate change in China: an empirical assessment based on long-term observations at different spatial scales (1981–2005). Agric. For. Meteorol. 150 (7–8), 1128–1137. https://doi.org/10.1016/j.agrformet.2010.04.013.

Zhang, J., Reid, J.S., Alfaro-Contreras, R., Xian, P., 2017. Has China been exporting less particulate air pollution over the past decade? Geophys. Res. Lett. 44. https://doi.org/10.1002/2017GL072617.

Zhang, T., Tao, L., Yue, X., Yang, X., 2017. Impacts of aerosol pollutant mitigation on lowland rice yields in China. Environ. Res. Lett. 12, 104003. https://doi.org/10.1088/1748-9326/aa80f0.

Zhang, H.Y., Cheng, S.Y., Li, J.B., Yao, S., Wang, X.Q., 2019. Investigating the aerosol mass and chemical components characteristics and feedback effects on the meteorological factors in the Beijing-Tianjin-Hebei region, China. Environ. Pollut. 244, 495–502. https://doi.org/10.1016/j.envpol.2018.10.087.

Zhao, B., Jiang, H., Gu, Y., Diner, D., Worden, J., Liou, K., Su, H., Xing, J., Garay, M., Huang, L., 2017. Decadal-scale trends in regional aerosol particle properties and their linkage to emission changes. Environ. Res. Lett. 12, 054021. https://doi.org/10.1088/1748-9326/aa6cb2.

Zheng, B., Tong, D., Li, M., Liu, F., Hong, C., Geng, G., Li, H., Li, X., Peng, L., Qi, J., Yan, L., Zhang, Y., Zhao, H., Zheng, Y., He, K., Zhang, Q., 2018. Trends in China's anthropogenic emissions since 2010 as the consequence of clean air actions. Atmos. Chem. Phys. 18, 14095–14111. https://doi.org/10.5194/acp-18-14095-2018.

Zhong, J., Zhang, X., Wang, Y., Liu, C., Dong, Y., 2018. Heavy aerosol pollution episodes in winter Beijing enhanced by radiative cooling effects of aerosols. Atmos. Res. 209, 59–64. https://doi.org/10.1016/j.atmosres.2018.03.011.

Zhong, J., Zhang, X., Wang, Y., Wang, J., Shen, X., Zhang, H., Wang, T., Xie, Z., Liu, C., Zhang, H., Zhao, T., Sun, J., Fan, S., Gao, Z., Li, Y., Wang, L., 2019. The two-way feedback mechanism between unfavorable meteorological conditions and cumulative aerosol pollution in various haze regions of China. Atmos. Chem. Phys. 19, 3287–3306. https://doi.org/10.5194/acp-19-3287-2019.

Zhou, L., Chen, X.H., Tian, X., 2017. The impact of fine particulate matter (PM2.5) on China's agricultural production from 2001 to 2010. J. Clean. Prod. 178, 133–141. https://doi.org/10.1016/j.jclepro.2017.12.204.

Zhuang, B., Wang, T., Liu, J., Che, H., Han, Y., Fu, Y., Li, S., Xie, M., Li, M., Chen, P., Chen, H., Yang, X., Sun, J., 2018. The optical properties, physical properties and direct radiative forcing of urban columnar aerosols in the Yangtze River Delta, China. Atmos. Chem. Phys. 18 (2), 1419–1436. https://doi.org/10.5194/acp-18-1419-2018.